Copyright © 2008. Reprinted from APPLIED PHYSICS LETTERS 93, 072903, 2008. Such permission of the American Institute of Physics does not in any way imply the American Institute of Physics endorsement of any of Institute of Microelectronics' products or services. Internal or personal use of this material is permitted. However, permission to reprint/republish this material for advertising or promotional purposes or for creating new collective works for resale or redistribution must be obtained from the American Institute of Physics by writing to Rights@aip.org.

The nature of dielectric breakdown

X. Li,[1,2] C. H. Tung,[1,a)] and K. L. Pey[2]
[1]*Institute of Microelectronics, A*STAR (Agency for Science, Technology and Research), 11 Science Park Road, Singapore Science Park II, Singapore 117685, Singapore*
[2]*Microelectronics Center, School of EEE, Nanyang Technological University, Nanyang Avenue, Singapore 639798, Singapore*

(Received 5 July 2008; accepted 1 August 2008; published online 20 August 2008)

Dielectric breakdown is the process of local materials transiting from insulating to conductive when the dielectric is submerged in a high external electric field environment. We show that the atomistic changes of the chemical bonding in a nanoscale breakdown path are extensive and irreversible. Oxygen atoms in dielectric SiO_2 are washed out with substoichiometric silicon oxide (SiO_x with $x<2$) formation, and local energy gap lowering with intermediate bonding state of silicon atoms (Si^{1+}, Si^{2+}, and Si^{3+}) in the percolation leakage path. Oxygen deficiency within the breakdown path is estimated to be as high as 50%–60%. © *2008 American Institute of Physics*.
[DOI: 10.1063/1.2974792]

Dielectric breakdown is a universal process that lies under a broad variety of natural phenomena, from corona discharge to thunder lightning, as well as man-made electrical devices such as laser printer and disruptive components in a circuit.[1] Mathematical models[2] have been made available to explain the randomness and fractal nature of a breakdown. Dielectric breakdown model typically describes the macroscopic behavior combining diffusion-limited aggregation with electric field for solids, liquids, and gases. Despite the success of the mathematical models, these phenomenological descriptions failed to reveal fundamental physical mechanism responsible for an insulating material transforming into a conductive path locally at the breakdown site. The lack of understanding on the physical process of a breakdown is largely due to the difficulties involved in determining and analyzing the microscopic breakdown path within the dielectric materials.

The experimental challenges pose two key difficulties to overcome. First, the nanoscale breakdown path needs to be accurately located and isolated for analysis. Depending on the analytical tools chosen, sample preparation plays an important role in the analysis process. Not only that the size of the breakdown path is only a few nanometers in diameter, but also the dielectric breakdown spot is buried underneath the electrode, such as metal line conductors and protective insulator coatings. Second, despite the efforts over the years,[3–5] the nature of a breakdown percolation path remains unknown today and there is no simple way to know whether the sample prepared contains the percolation path. Since the percolation path is typically invisible under the analytical tools used, a clear signature or nanomarker must be present to aid the navigation and eventually confirmation of the existence of a percolation path.

To overcome the above difficulties, a proper sample structure must be used to aid and identify the breakdown location for sample preparation, and subsequently to navigate to the breakdown spot even though the breakdown path is invisible under a microscope. The metal-oxide-semiconductor transistor is an ideal structure for dielectric breakdown studies. The electrical behaviors of the dielectric layer are easily characterized using the four electrodes of the transistor. The size of the transistor can be selected to be as small as a typical transmission electron microscopy (TEM) sample thickness so that a breakdown spot can be obtained. Moreover, dielectric breakdown due to electrical stressing or testing can trigger damages to the physical integrity and microstructure in the surrounding of the breakdown spot of the device.[6,7] It was demonstrated that dielectric breakdown induced epitaxy (DBIE) marks an important physical signature of breakdown location where the invisible percolation path can be located unambiguously.[8,9] Figure 1 shows the TEM and scanning transmission electron microcopy (STEM) cross-sectional views of a four-electrode transistor with a breakdown in the silicon dioxide dielectric layer. The electrical location of the leakage path is at the center of the channel length ($0.5L$, where L is the effective channel length) measured using a current separation method.[10] The high resolution TEM (HRTEM) lattice image, Fig. 1(b), shows the 2 nm gate oxide at the breakdown location with a DBIE identified and delineated. Figure 1(c) is the corresponding STEM annular dark field (ADF) image. As shown in Figs. 1(b) and 1(c), the percolation path directly atop of DBIE is invisible in ordinary TEM/STEM imaging modes.

Subsequently, electron energy loss spectrometry (EELS) analysis was performed at the breakdown location (i.e., above the DBIE), in an attempt to analyze the chemical nature of the percolation path. Figure 2 illustrates the close-up view of the sample configuration and beam-sample interaction. STEM/EELS spectra were collected using point-to-point vertical scan across the dielectric layer at the breakdown site and at the nonbreakdown site. Figure 3 shows the background corrected Si $L_{2,3}$ edge spectra from three different positions, including a spectrum at a nonbreakdown oxide/Si interface (short-dashed line) for comparison. The spectrum for a nonbreakdown (normal) gate oxide (dash-dotted line) has a Si^{4+} bonding characteristic between 106 and 108 eV,[11] with a shoulder peak extended down to 100 eV. The additional energy states that appeared below 106 eV are attributed to the delocalized signals[12,13] from the interface suboxide,[11] which can also be seen in the spectrum from

a)Author to whom correspondence should be addressed. Tel.: +65-6770-5370. FAX: +65-6770-1914. Electronic mail: chihhang@ime.a-star.edu.sg.

 © 2008 American Institute of Physics

Author complimentary copy. Redistribution subject to AIP license or copyright, see http://apl.aip.org/apl/copyright.jsp

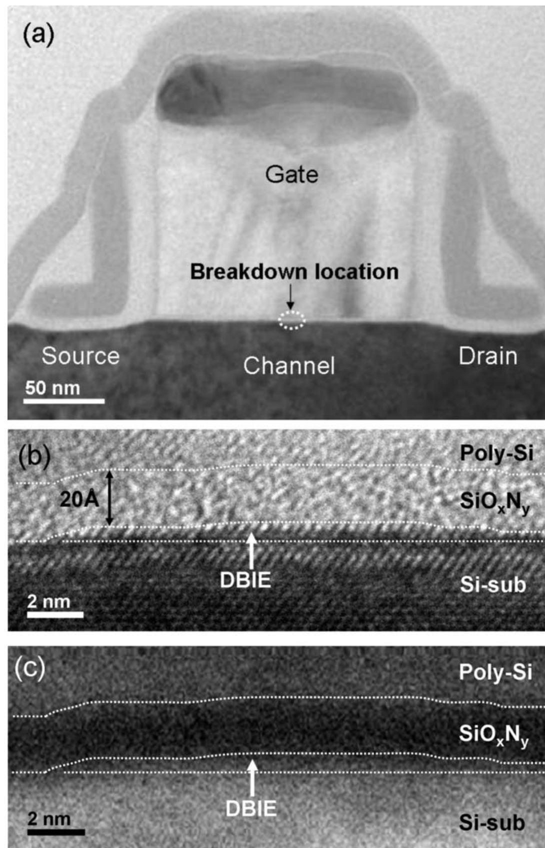

FIG. 1. TEM/STEM cross-sectional views of a transistor with dielectric breakdown. (a) Low magnification TEM cross-sectional image of a failed transistor ($W \times L = 0.15 \times 0.2\ \mu m^2$) after electrical stress $V_{gstress} = 4.3$ V (step 1) and 3.2 V (step 2) with gate compliance current limit $I_{gl} = 10\ \mu A$ (step 1) and 200 μA (step 2). The electrical stress is performed at room temperature while keeping other electrodes grounded. The breakdown location measured electrically is at the center of the channel length ($0.5L$, where L is the effective channel length), as highlighted in the dotted circle. (b) HRTEM lattice image of the breakdown location. DBIE is marked and the oxide area on top of the DBIE bump is displayed. The gate oxide is a 2.0 nm nitrided amorphous SiO_2 (N%~3%). (c) ADF image of the breakdown location. It shows no difference for the oxide area on top of the DBIE bump as compared to the nonbreakdown oxide.

the oxide/substrate interface. The Si $L_{2,3}$ edge for the breakdown oxide (solid line) as compared to the nonbreakdown oxide (dash-dotted line) shows reduced intensities at 108 eV (Si^{4+}) but increased intensities between 100 and 105 eV (Si^0 and intermediate oxidation states Si^{1+}, Si^{2+}, and Si^{3+}). From our momentum resolved density of states (DOS) calculation (not shown) using all electron density functional theory performed on α-quartz SiO_2, the effect of oxygen vacancy will lower the s-states[14] at 108 eV but create more s - and d-states

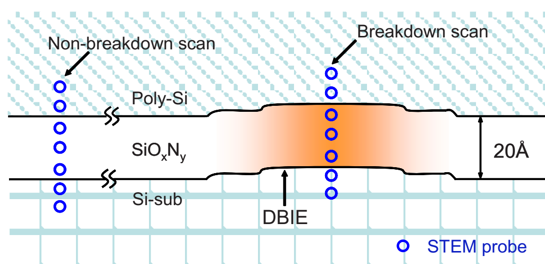

FIG. 2. (Color online) Schematic of the STEM-EELS point-to-point scan across the gate dielectric layer at breakdown and nonbreakdown locations. The percolation path is located at the oxide areas on top of the DBIE.

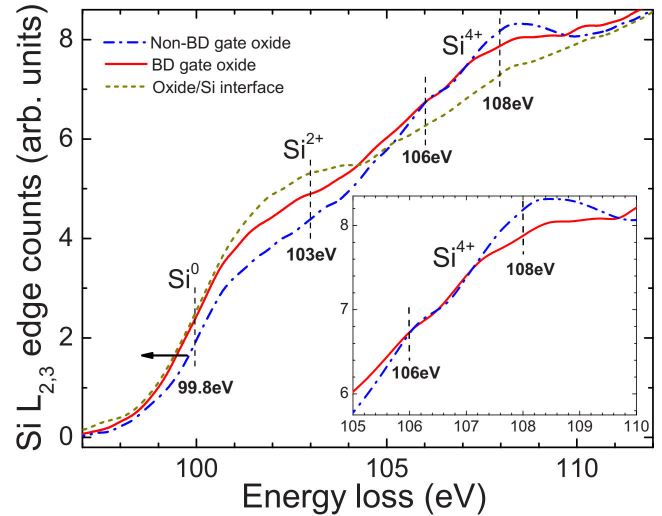

FIG. 3. (Color online) The background corrected Si $L_{2,3}$ edge spectra from breakdown (solid) and nonbreakdown (dash-dotted) gate oxides and oxide/Si interface (short-dashed). The breakdown oxide shows less Si^{4+} signals at 108 eV but more Si^0 and Si intermediate oxide state signals below 106 eV as a result of oxygen deficiency. The inserted figure shows the enlarged plot from 105 to 110 eV for breakdown and nonbreakdown oxides. The arrow indicates the edge onset lowering of 0.6 eV for breakdown oxide. The EELS measurements were performed on a FEI-TITAN 300 kV TEM/STEM. The probe size was set to be approximately 4 Å in diameter and the EELS energy resolution is 1.5 eV with a 0.3 eV/channel dispersion (600 eV energy range). The spectra collected from the central region of the gate oxide at breakdown and nonbreakdown locations are extracted for comparison.

below 106 eV, which agree with the current experimental observations. The obvious increase in the EELS intensities from 100 to 105 eV suggests the presence of Si atoms coordinated with less than four oxygen atoms (i.e., suboxide) and possible Si nanoscopic clustering.[11] The edge onset (~100 eV) for the breakdown oxide is shifted to a lower energy of about 0.6 eV (indicated by arrow), possibly due to local conduction band offset lowering.[15]

The O K edge core-loss from the bulk oxide (solid), and the nonbreakdown (dashed) and breakdown (dash-dotted) gate oxides are presented in Fig. 4. The first absorption peak at 537.8 eV as shown for the bulk oxide (solid line) is originated from the multiple scattering[16] of the ejected O 1s electron to its six second-nearest neighboring O atoms (first O shell).[17] It can be directly related to the local conduction band electronic properties.[18] The spectrum for the nonbreakdown gate oxide (dashed line) has the same absorption peak at 537.8 eV. However, the rising portion of the edge onset at ~530 eV is shifted to a lower energy as compared with the bulk oxide (solid line). This is likely due to the delocalized scattering from the interface suboxide, which lowers the conduction band minimum.[17,18] The reduced edge onset is also observed for the breakdown gate oxide (dash-dotted line). It is thus difficult to distinguish, from the O K edge study for ultrathin gate oxide with signal delocalization, if the breakdown oxide has induced a local conduction band lowering. Comparing the first peak position between the nonbreakdown and breakdown gate oxides, the peak position shifts from 537.8 to 536.3 eV upon breakdown. It is believed that such shift is a result of conduction band p-DOS redistribution within the percolation path. Note that a redshift (to a lower energy of about 4 eV) is observed in the second absorption peak (~560 eV) for both breakdown and nonbreak-

Author complimentary copy. Redistribution subject to AIP license or copyright, see http://apl.aip.org/apl/copyright.jsp

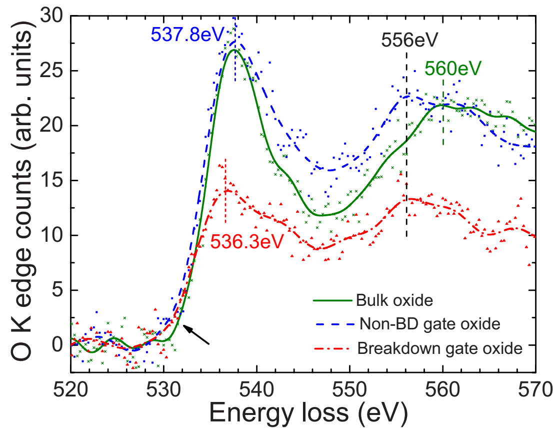

FIG. 4. (Color online) The background corrected O K edge spectra measured from bulk oxide (solid) and breakdown (dash-dotted) and nonbreakdown (dashed) gate oxides. The first peak position (537.8 eV) shifts to a lower energy (536.3 eV) as a result of conduction band p-state redistribution. The arrow indicates the edge onsets for nonbreakdown gate oxide is lowered as compared to the bulk oxide. Si/O ratio was quantified using the edge intensity integrated from 99 to 129 eV for Si L and from 532 to 542 eV for O K. The missing of O atoms at the breakdown area is reflected from the lowered intensities (dash-dotted line). The ratio for the breakdown oxide is $SiO_{0.9}$ normalized using the nonbreakdown oxide as SiO_2. However, this value is underestimated due to the difference between the percolation path diameter and the TEM sample thickness.

down gate oxides. This shift originates from the presence of stretched O–O bonds[19–21] in ultrathin gate oxide and was not affected by the breakdown.

The breakdown gate oxide as compared with the nonbreakdown gate oxide shows significantly lower O K core-loss signals. The decrease in the intensity arises from the missing O atoms[17] at the breakdown site. The deficiency of O atoms within the breakdown SiO_2 can be calculated using the core-loss signal intensities.[22] The Si/O ratios are calculated using the respective edge intensities for the breakdown oxide while using the nonbreakdown oxide calibrated as SiO_2 with $Si/O=1/2$. The oxygen deficiency within the breakdown path calculated using this approach is as high as 50%–60%. From the results shown in Figs. 3 and 4, the intensity change in the Si $L_{2,3}$ edge is minimum compared with the O K edge. This suggests that oxygen depletion, instead of silicon accumulation, is the chemical and atomistic mechanism responsible for the ultrathin SiO_2 oxide breakdown path formation.

In summary, the site-specific structural analysis using STEM-EELS was performed on dielectric breakdown percolation path. The results show that oxygen deficiency is the key signature for the structural change at a molecular level in the breakdown path. Chemical bond breakage and the local Joule heating due to large current surging through the percolation path are believed to be the main driving forces leading to the oxygen dissociation and washout. Since different numbers of oxygen atoms at the nearest neighbors result in different local energy gaps, it is believed that the local energy gap at the breakdown path could have collapsed after the removal of oxygen atoms and there is a rearrangement of local atomic structures. The presence of a nanoscopic conduction path is therefore possible in the highly oxygen deficient breakdown oxide. Such understanding will be critical to the development of dielectric systems made from polymeric, ceramics, low-κ, and high-κ materials for future device applications.

We thank G. Zhang and V. L. Lo for technical discussions and sample preparation, and Chartered Semiconductor Manufacturing for providing the samples. This work was supported by Ministry of Education (MOE) Grant Nos. T206B1205 and NTU RGM 33/03.

[1]D. B. Strukov, G. S. Snider, D. R. Stewart, and R. S. Williams, Nature (London) **453**, 80 (2008).
[2]L. Niemeyer, L. Pietronero, and H. J. Wiesmann, Phys. Rev. Lett. **52**, 1033 (1984).
[3]R. Degraeve, G. Groeseneken, R. Bellens, M. Depas, and H. E. Maes, Tech. Dig. - Int. Electron Devices Meet. **1995**, 863.
[4]J. W. McPherson and H. Mogul, J. Appl. Phys. **84**, 1513 (1998).
[5]J. W. McPherson, J. Appl. Phys. **99**, 083501 (2006).
[6]M. K. Radhakrishnan, K. L. Pey, C. H. Tung, W. H. Lin, and S. H. Ong, Tech. Dig. - Int. Electron Devices Meet. **2001**, 857.
[7]K. L. Pey, C. H. Tung, M. K. Radhakrishnan, L. J. Tang, and W. H. Lin, Tech. Dig. - Int. Electron Devices Meet. **2002**, 163.
[8]C. H. Tung, K. L. Pey, W. H. Lin, and M. K. Radhakrishnan, IEEE Electron Device Lett. **23**, 526 (2002).
[9]C. H. Tung, K. L. Pey, L. J. Tang, M. K. Radhakrishnan, W. H. Lin, F. Palumbo, and S. Lombardo, Appl. Phys. Lett. **83**, 2223 (2003).
[10]B. Kaczer, IEEE Trans. Electron Devices **49**, 507 (2002).
[11]P. E. Batson, Nature (London) **366**, 727 (1993).
[12]R. F. Egerton, Ultramicroscopy **107**, 575 (2007).
[13]D. A. Muller and J. Silcox, Ultramicroscopy **59**, 195 (1995).
[14]L. A. J. Garvie, P. Rez, J. R. Alvarez, P. R. Buseck, A. Craven, and R. Brydson, Am. Mineral. **85**, 732 (2000).
[15]P. E. Batson, Ultramicroscopy **59**, 63 (1995).
[16]P. Rez, J. Bruley, P. Brohan, M. Payne, and L. A. J. Garvie, Ultramicroscopy **59**, 159 (1995).
[17]D. A. Muller, T. Sorsch, M. Moccio, F. H. Baumann, and K. Evans-Lutterodt, G. Timp, Nature (London) **399**, 758 (1999).
[18]J. B. Neaton, D. A. Muller, and N. W. Ashcroft, Phys. Rev. Lett. **85**, 1298 (2000).
[19]Z. W. Yuan, S. Csillag, M. A. Tafreshi, and C. Colliex, Ultramicroscopy **59**, 149 (1995).
[20]Y. Ito, D. Winkler, H. Jain, and D. B. Williams, J. Non-Cryst. Solids **222**, 83 (1997).
[21]N. Jiang and J. C. H. Spence, Ultramicroscopy **106**, 215 (2006).
[22]K. A. Mkhoyan, J. Silcox, A. Ellison, D. Ast, and R. Dieckmann, Phys. Rev. Lett. **96**, 205506 (2006).

Author complimentary copy. Redistribution subject to AIP license or copyright, see http://apl.aip.org/apl/copyright.jsp